Faria S.H. 2018. Slip-band distributions and microstructural fading memory beneath the firn--ice transition of polar ice sheets. MECHANICS RESEARCH COMMUNICATIONS. 94. 95-101. DOI (10.1016/j.mechrescom.2018.09.009).

Slip-band distributions and microstructural fading memory beneath the firn–ice transition of polar ice sheets*

Sérgio Henrique FARIA
Basque Centre for Climate Change (BC3), 48940 Leioa, Spain
IKERBASQUE, Basque Foundation for Science, 48013 Bilbao, Spain

September 27, 2018

Abstract

The Antarctic Ice Sheet is a continental ice mass with circa 23 million gigatons of ice, which represent roughly 67 % of world's freshwater supply. This colossal mass of ice is by no means static, as the old ice slowly creeps under its own weight towards the ocean, while new ice is continually formed through the sintering of snow deposited on the ice sheet surface. A crucial role in this metamorphism is played by firn, which is the porous material in an intermediate state between the granular snow and the solid polycrystalline ice. Understanding the snow–firn–ice metamorphism is essential not only for a precise determination of the mechanical (creep) properties of polar ice, but also for comprehending the formation and decay of climate proxies widely used in ice-core studies. This work investigates the transition from firn to ice through the spatial and directional distributions of slip bands in bubbly ice. The analysis of high-resolution micrographs of ice sections extracted from the EPICA-DML Deep Ice Core allows us to identify a clear influence of strain-induced anisotropy (viz. c-axis preferred orientations) on the evolution of slip-band inclinations in deep bubbly ice. In contrast, we discover an unanticipated behaviour of slip bands in shallow bubbly ice, which prompts the introduction of the hypothesis of *microstructural fading memory* and the definition of a *stabilization zone* that may penetrate hundreds of metres into the bubbly ice. Within this stabilization zone, highly localized concentrations of strain energy and internal stresses once generated by force chains in the ancient firn are gradually redistributed by the newly formed bubbly-ice microstructure. We show that this hypothesis is compatible with the localized dynamic recrystallization episodes observed in polar firn (even at temperatures close to -45 °C), and it may also explain the sluggish rotation of c-axes observed in the upper hundreds of metres of polar ice sheets.

key-words: Antarctica; Dronning Maud Land; ice; firn; snow; slip band; microstructure; force chain; heterogeneous deformation; internal stress; stored strain energy; recrystallization; recovery; ice flow; polycrystal

1 Introduction

With an average thickness close to 2 km (and in many places surpassing the 3 km mark), the Antarctic Ice Sheet covers a continental area larger than 13×10^6 km^2. This amounts to astonishing 23 million gigatons of ice (or 25×10^6 km^3, including ice shelves), which represent roughly 67 %

*Dedicated to my mentor and friend, Kumiko Goto-Azuma, on occasion of her 60th birthday.

of world's freshwater supply and a potential contribution to global sea-level rise of 58 m (Lemke et al., 2007; Vaughan et al., 2013). Such a colossal mass of ice is by no means static. Old ice slowly creeps under its own weight towards the ocean, while new ice is formed through the sintering of snow that is continually deposited on the ice sheet surface.

As it occurs with most crystalline solids, ice may undergo *creep* (viz. visco-plastic deformation) at rather low stresses, provided that its temperature is higher than roughly half of its pressure melting point (Durham et al., 2001; Petrenko and Whitworth, 1999). Seeing that this condition is fulfilled anywhere on Earth's surface, it should be no surprise that glaciers and ice sheets creep under their own weight. Even though the creep of such large ice masses is an expected phenomenon, its microscopic mechanisms have been challenging glaciologists for decades. In particular, a fundamental feature of the micro-mechanics of ice is its exceptional propensity to form *slip bands*, which are characteristic, microscopic fringes visible within certain ice grains or crystals undergoing simple shear (Hobbs, 1974; Nakaya, 1958). Considering that such slip bands are microscopic expressions of *basal slip* (viz. simple shear along a particular family of crystallographic planes, called *basal planes*) within an ice grain, we conclude that the occurrence of these fringes depends not only on the macroscopic deformation regime, but also on the crystalline properties of the grain and its interactions with neighbours.

The neighbourhood of a particular ice grain is mainly defined by the positions, crystalline orientations, shapes and sizes of the surrounding grains, which combined describe the local *orientation stereology* (Bunge and Schwarzer, 2001; Faria et al., 2014b, 2018). Under this perspective, the current neighbourhood of an ice grain is in fact a fading record of the local orientation-stereology history (Faria and Kipfstuhl, 2005), which begins with the deposition of snow crystals on the glacier or ice-sheet surface, and develops through the metamorphism of snow into firn and ice. Such a record is evanescent because it is gradually obliterated by thermomechanical processes of deformation, recovery, and recrystallization (following Faria et al. 2014b, 2018, the terms *recovery* and *recrystallization* are used here in a wide sense, including static and dynamic processes of structural change, like grain growth, grain boundary migration, and subgrain rotation). While ice microstructural changes directly related to deformation (e.g. crystalline lattice rotation, grain elongation, etc.) are relatively well understood and reproducible by models (Alley, 1988; Azuma, 1994; Azuma and Higashi, 1985; Faria et al., 2002; Gödert and Hutter, 1998; Placidi et al., 2010), rates of recovery and recrystallization of natural firn and ice are largely unknown (Faria et al., 2014b; Placidi et al., 2004). This lack of knowledge severely impairs the modelling of ice microstructure evolution and consequently limits the current predictive power of ice flow models and the interpretations of ice-core climate proxies.

This work aims to help clarifying the roles played by recovery and recrystallization in the fading memory of the local orientation stereology of polar firn and ice, therefore paving the way to a future quantification of these thermodynamic processes. This objective is achieved through the analysis of the orientation distributions of slip bands, which are identified in high-resolution, microscopic images of ice sections extracted from eight distinct depths of the EPICA-DML Deep Ice Core, from the EPICA (European Project for Ice Coring in Antarctica) drilling site in Dronning Maud Land (DML), Antarctica.

Precise definitions of the technical terms used in this work can be found in the glossaries presented by Faria et al. (2014b, 2018). The following section introduces the most fundamental concepts and put them into the context of the current study.

2 Fundamental Concepts

Under the natural conditions typically found on Earth's surface, ice occurs in the ordinary hexagonal form named *ice Ih*. With an atomic packing factor of less than 34 %, ice Ih has a rather open, wurtzite-like crystalline lattice (Evans, 1976; Hobbs, 1974), which is characterized by oxygen ions arranged in layers (called *basal planes*) of "puckered" hexagonal rings piled in an alternate sequence of mirror images normal to the axis of optical and crystallographic (hexagonal) symmetry of the crystal, viz. the *c axis*. Hydrogen nuclei (protons) remain statistically distributed in the oxygen lattice, building covalent and hydrogen bonds along the lines joining pairs of oxygen ions (Bernal and Fowler, 1933; Pauling, 1935). This *proton disorder* plays a fundamental role in ice plasticity, as it affects the motion of the main agents of plastic deformation of ice: *dislocations* (Glen, 1968, 1974; Petrenko and Whitworth, 1999).

Experience shows that the plasticity of monocrystalline ice is strongly anisotropic, with ice single crystals deforming very readily when the applied shear stress acts on the basal plane (Duval et al., 1983; Hobbs, 1974), through a process called *basal slip* and epitomized more than a century ago by McConnel's (1890) "deck of cards" metaphor. This phenomenon was later beautifully illustrated by Nakaya (1958), who used shadow photography to reveal *slip bands* in deformed monocrystalline ice bars. Not long after, Bryant and Mason (1960) found grouped etch pits and channels along slip bands in resin replicas of deformed ice monocrystals, corroborating the prevalent hypothesis that slip bands consisted of microscopic layers with high density of dislocations undergoing basal slip. In contrast to laboratory tests, the optical observation of slip bands in polar ice turns out to be much more challenging, because of the very low strain rates typical of ice-sheet flow. Nevertheless, modern microscopy techniques, like the microstructure mapping (μSM) method adopted in this study, have revealed that slip bands are indeed a common feature also of polar ice (Faria and Kipfstuhl, 2004; Kipfstuhl et al., 2006; Wang et al., 2003).

3 Methods

All ice samples investigated here stem from the EPICA-DML Deep Ice Core (Faria et al., 2018): a 2774.15 m long ice core extracted from the EPICA (European Project for Ice Coring in Antarctica) drilling site at Dronning Maud Land (DML), Antarctica (75°00'09"S, 00°04'06"E, 2892 m a.s.l.). Eight ice samples were selected, consisting of vertical thick sections ($\approx 50 \times 100 \times 5$ mm) cut lengthwise the EPICA-DML Deep Ice Core at roughly 100 m intervals. Details of the samples are described in Table 1. Following the usual convention of the ice-core physical-properties community, all depths are *rounded down*. The sampling approximately covered the upper 850 m of ice, i.e. the last 16 ka BP (Ruth et al., 2007). The reason to chose this depth range is threefold, being mainly related to changes in the physical properties of the ice core, as well as changes in the ice flow and climatic conditions in Antarctica, namely:

1. Below 800 m depth commences the EPICA-DML bubble–hydrate transition zone, where air bubbles are no longer thermodynamically stable and start transforming themselves into air hydrates (Bendel et al., 2013; Faria et al., 2010, 2014a; Ueltzhöffer et al., 2010).

2. Even though no well-defined "brittle zone" has been discerned in the EPICA-DML site, the ice-core quality between 800 m and 1000 m depth was conspicuously lower (Faria et al., 2010, 2018; Wilhelms et al., 2014).

3. The onset of the Antarctic Ice Sheet retreat from its Last Glacial maximum extent is estimated to have occurred not longer after 16 ka BP (Clark et al., 2009).

Ice samples were prepared and analysed through the method of *Microstructure Mapping* (µSM), which is essentially a digital form of optical microscopy (Faria and Kipfstuhl, 2004; Kipfstuhl et al., 2006; Wang et al., 2003; Weikusat et al., 2009). The µSM method consists of a digital video camera with automatic gain control mounted on an optical microscope equipped with a computer-controlled xy-stage. The microscope automatically scans the whole sample, mapping a variety of microstructural features inside the ice (ranging from microinclusions and dislocation walls to air bubbles, clathrates, and slip bands) with a microscopic resolution of ca. 3 µm per pixel. Up to 1800 photomicrographs may be needed to reconstruct a high-resolution digital mosaic image of a 50×100 mm section. Micrographs are usually taken in transmitted light, with a standard size of 2.5×1.8 mm and a typical overlapping of ca. 0.5 mm, which facilitates the later reconstruction of the full mosaic image through the matching of neighbouring micrographs.

All µSM micrographs analysed in this work are freely available at the Pangaea digital data library (Kipfstuhl, 2007).

The preparation of µSM samples follows the usual procedures for ice microscopy (Kipfstuhl et al., 2006; Weikusat et al., 2009). Band saws and microtomes are respectively used for cutting and polishing the sections. Clear surfaces are achieved by exposing the polished section to the free atmosphere: sublimation smooths the ice surface through the removal of superficial imperfections (e.g. microtome scratches), while it simultaneously highlights the sites where grain boundaries and other high-energy structures meet the surface, through the formation of characteristic thermal-etching grooves and pits (Hobbs, 1974; Kuroiwa and Hamilton, 1963; Mullins, 1957; Nishida and Narita, 1996). A sublimation time varying between half an hour and half a day is usually necessary to obtain a clear surface, with well-developed grain-boundary grooves. This sublimation time strongly depends on the conditions of temperature, humidity, and air circulation above the sample.

After the first (lower) surface of the section is sufficiently clear, it is sealed off with a thin film of silicone oil and frozen onto a glass plate. The second (upper) surface is treated in the same manner, but it is sealed off with silicone oil and glass only after the first surface scan is completed, in order to optimize the quality of the µSM images. Once both surfaces are sealed, further scans are often performed with the microscope focused inside the section, in order to map microstructural features not related to the etched surface, like air bubbles and hydrates, microinclusions, and slip bands. Examples of µSM micrographs showing real and "fake" slip bands are presented in Fig. 1.

The portability of the µSM method permits the mapping of fresh ice sections in the field, while drilling is ongoing. This is crucial for minimizing the effects of recrystallization, recovery and post-drilling relaxation of the ice microstructure. Under optimal conditions, the mapping of a complete section ($50 \times 100 \times 5$ mm) takes about one hour and can be accomplished as early as a few hours after core extraction.

Analysis of the µSM micrographs was performed with the open-source software *Fiji–ImageJ* (Schindelin et al., 2012). Circa 12,000 micrographs were manually analysed, through the identification of grain and subgrain boundaries, dislocation walls, and slip bands. Special care was taken at the overlapping regions between micrographs. Every time a grain with a set of parallel slip bands was manually identified, the software determined the position and inclination of the set, labelled it, and recorded the information in a spreadsheet. Thus, as a rule, each slip-band-inclination data point corresponds to the set of slip bands in an individual grain. An exception was made for some very large grains with well-defined slip bands: in such cases, the grain was decomposed into sectors of size comparable with the average grain size, and each sector was measured separately. The angular precision of the measurements was of approximately 2 degrees.

Automatic analysis of slip bands was not possible, because the correct identification of slip bands is exceptionally difficult (cf. Fig. 1): software and untrained eyes often confuse them with defocused surface irregularities (e.g. sublimation grooves), or with occasional optical aberrations (caused e.g. by some internal grain-boundary edges). Therefore, to date, the manual identification of slip bands by a judicious and experienced specialist in ice microscopy and μSM is still the most reliable procedure. Hopefully, new techniques of machine learning applied to image analysis may enable the automation of these procedures in the near future.

It should be noted that firn samples have not been analysed in this study. Whereas the μSM method has already been successfully employed to investigate the microstructure of firn (Faria et al., 2010, 2014b; Kipfstuhl et al., 2009), such investigations were restricted to reflected-light microscopy of sublimation grooves (of grain and subgrain boundaries) on the ice surface. The reason for this restriction is that firn is not transparent as ice: the porous structure of firn permeates through the whole section, scattering the transmitted light that would be necessary to reveal internal structures inside the ice section, like slip bands.

4 Results

Slip bands were identified and classified according to their inclinations with respect to the horizontal plane. Two remarks are relevant in this regard:

Remark 1: Ice cores drilled to date (including the EPICA-DML Deep Ice Core) have arbitrary azimuths (Faria et al., 2018; Weikusat et al., 2017), and consequently, so have also their vertical sections.

Remark 2: Owing to their faint nature and stacked arrangement, slip bands in polar ice are best discerned if they are nearly perpendicular to the view plane, i.e. the section's surface (misorientation $< 10°$; Kipfstuhl et al. 2006).

From Remark 1, it follows that only the slip band's *apparent dip angle* (viz. perceived angle of inclination) can be determined. In general, the apparent dip angle represents a lower bound of the *true dip angle* (viz. maximum angle of inclination). Nevertheless, Remark 2 implies that discernible slip bands usually have apparent dip angles similar to their respective true dip angles. Be that as it may, here we stick to the expression "apparent dip angle", in order to stress two important facts: (i) the apparent and true dip angles may not be identical; (ii) the azimuth of a vertical section, and consequently the slip band's *dip direction*, is unknown.

Figure 2 displays four examples of apparent-dip-angle distributions of slip bands, with an accuracy of five degrees. The evolution of these distributions with depth, and consequently with age, is clearly visible. The most obvious feature of the whole depth interval is a net increase in the fraction of *low-angle* ($< 30°$) slip bands at the expense of *mid-angle* (between 30° and 60°) and *high-angle* ($\geq 60°$) slip bands. Closer inspection reveals, however, a somewhat more complex development: down to a *reversal zone* at (415 ± 60) m depth, there is actually a *decrease* in the frequency of low-angle slip bands, which is simultaneously compensated by an *increase* in the frequency of mid-angle slip bands. In contrast, at some point within that reversal zone this process is reversed and the mid-angle slip bands start to disappear, while low-angle slip bands gradually increase in number. These observations are illustrated in Fig. 3, which shows the depth evolution of low-, mid-, and high-angle slip bands in all eight sections analysed in this study. Notice also that the frequency of high-angle slip bands decreases through the whole depth range (94–854 m) in a rather linear fashion.

5 Discussion

The observation that the frequency of high-angle slip bands decreases monotonically with depth throughout the studied interval (94–854 m) should be no surprise for those aware of the ice-flow features at the EPICA-DML site: the decrease can be explained as a direct consequence of the developing strain-induced anisotropy of polycrystalline ice in that region (viz. lattice preferred orientations, so-called "fabric"). The EPICA-DML drilling site lies on an ice ridge. Therefore, by considering the general rule that the ice flow in the upper part of a stationary ice sheet can be roughly described by its surface down-slope combined with the ubiquitous vertical compression due to the overburden of continual snow accumulation, we conclude that the large-scale flow in the upper thousand metres at EPICA-DML has a triaxial character, dominated by horizontal extension across the ridge ($\sim 10^{-4}$ a^{-1}), vertical compression ($\sim 10^{-4}$ a^{-1}), and a slight horizontal compression rate along the ridge (one or more orders of magnitude smaller than the other two rates). These strain-rate estimates are compatible with airborne surface-velocity observations, numerical simulations, and microstructure analysis (Faria et al., 2014b, 2018; Steinhage, 2001; Weikusat et al., 2017).

The anisotropic c-axis orientation distribution induced by this kind of deformation may be called a "vertical great-circle girdle with a vertical maximum," which means that the c axes tend to reorient themselves with increasing depth away from the (horizontal) principal axis of extension and towards the principal axes of compression—especially the stronger vertical one. Accordingly, this means that the basal planes have an increasing tendency to become tangent to the principal axis of extension, as if they were arranging themselves on the elliptical cylindrical surface of a fictitious "horizontally flattened tube." Therefore, irrespective of the orientation of the vertical section, most basal planes in deeper samples should be at low angles with respect to the horizontal, and so should also be the most frequently observed slip bands.

Whereas the above description explains the monotonic decrease with depth in the frequency of high-angle slip bands, the observation that this decrease is approximately linear is unanticipated, especially if we consider the strongly non-linear evolution of the other two dip classes. This is a matter that deserves further investigation in the near future.

In contrast to the relatively straightforward explanation for the evolution of high-angle slip bands, the evolution of low- and mid-angle slip bands is much less trivial. Two contrasting behaviours are observed above and below a reversal zone identified at (415 ± 60) m depth. Below this reversal zone, the evolution of low- and mid-angle slip bands follows the expected behaviour, with mid-angle slip bands gradually giving way to an increasing number of low-angle slip bands. Such a behaviour is "expected" in the sense that it can be explained with the same arguments already used to explain the progressive reduction in the frequency of high-angle slip bands. On the other hand, in the shallower depths above the reversal zone, the frequencies of low- and mid-angle slip bands behave in the opposite way: the fraction of low-angle slip bands observed at shallow depths gradually decreases with depth down to the reversal zone. Likewise, the fraction of mid-angle slip bands observed at shallow depths progressively increase in importance towards the reversal zone. These two contrasting behaviours clearly cannot be explained with the arguments about induced anisotropy invoked for high-angle slip bands and for the region below the reversal zone. Another explanation is needed.

The reason for discarding the induced-anisotropy explanation in the case of shallow bubbly ice is obvious: polycrystalline ice in the upper 450 m depth of the EPICA-DML site is nearly isotropic (Weikusat et al., 2017). This is, however, also the reason why the behaviour of low- and mid-angle slip bands in the shallow ice above the reversal zone seems counter-intuitive: the macroscopic strain rate anywhere in the upper 1000 m of EPICA-DML is essentially the same—viz. the triaxial regime already described—and this fact combined with the near-isotropy of shallow ice implies that the most probable slip bands in the upper hundreds of metres should be at mid-angles, because basal planes at such inclinations can bear the largest resolved shear stresses from the macroscopic triaxial load (Asaro, 1983; Faria and Kipfstuhl, 2004; Placidi et al., 2006).

Thus, it turns out that the crucial question about the evolution of slip bands in shallow polar ice at the EPICA-DML site is: *why do the frequency of mid-angle slip bands in the uppermost few hundred metres* increase *with depth down to the reversal zone?* In a reciprocal formulation: *why do the frequency of low-angle slip bands in the uppermost few hundred metres* decrease *with depth down to the reversal zone?*

Here we propose an answer to the above question in the form of a novel hypothesis of *microstructural fading memory*. In a few words, its fundamental idea is that the shallow bubbly ice inherits some microstructural imprints and localized strain energy from the former granular and porous structures of snow and firn, which affect the distribution of slip bands at shallow depths. Such inherited force-chain relics gradually evanesce with time and depth, under the action of dynamic recovery and recrystallization, and the redistribution of internal stresses.

More precisely, it is well known that the sintering of granular snow and porous firn into solid, polycrystalline bubbly ice generates an intricate network of *force chains*, viz. more or less stable, load-bearing trains of grains within the firn skeleton (Brown, 1980; Gubler, 1978; Kry, 1975; Scapozza and Bartelt, 2003; von Moos et al., 2003; Wakahama, 1960). Such force chains have the ability to transfer, modify, and break down the applied macroscopic stress into a series of complex and seemingly uncorrelated microscopic internal stresses, which give rise to strong strain heterogeneities in clusters of grains that undergo large amounts of strain accommodation, facilitated by the pore space. These internal stresses can sometimes be so intense that they may cause localized dynamic recrystallization in cold firn (down to -45 °C), a phenomenon first observed by Kipfstuhl et al. (2009) and theoretically explained by Faria et al. (2014b).

Within the context of this study, a fundamental feature of the microscopic internal stresses generated by force chains in firn is that the directions and intensities of their principal stresses may vary wildly among neighbouring clusters of grains on the micro- and meso-scales, and may also considerably differ from the macroscopic principal stresses related to the large-scale ice flow. Seeing that slip bands form and evolve in ice in response to local, microscopic principal stresses (through their projections onto the basal planes of the crystalline ice lattice as resolved shear stresses), we conclude that the orientation distribution of slip bands in polar firn on the mesoscale ($\sim 10^{-1}$ m) should express this diversity of microscopic principal stresses through a more random distribution of slip-band orientations than it would be expected for a solid piece of isotropic polycrystalline ice subjected to a well-defined triaxial load.

The hypothesis of microstructural fading memory asserts that the most intense and stable force chains in firn should produce highly localized concentrations of strain energy around trains of load-bearing grains that remain partially active and preserved, together with some of the strongest slip bands, in the microstructure of shallow bubbly ice beneath the firn–ice transition (pore close-off depth). Such remaining slip bands and trains of grains represent relics of the former firn structure, which gradually lose influence on the microstructure of shallow ice and decay through the redistribution of internal stresses and the action of dynamic recovery and recrystallization (including grain growth). Indeed, the slip-band distributions observed in the EPICA-DML sections from 94, 205 and 355 m depth express precisely this phenomenon: they describe the gradual transition from a nearly-random orientation distribution of slip bands at 94 m depth to a mid-angle-dominated distribution characteristic of solid, polycrystalline ice subjected to a well-defined triaxial load.

The depth range in which all these decay processes take place and the memory of the ancient firn microstructure fades away defines the *stabilization zone*, which coincides with the shallow bubbly ice zone ranging from the pore close-off depth down to the end of the slip-band reversal zone identified in this work. It is in the stabilization zone that the last manifestations of the highly heterogeneous deformation nature of porous firn give way to the more homogeneous deformation regime of solid polycrystalline ice. This is valid not only for the distribution of slip bands, but also for other microstructural features, including the orientation of *c*-axes, as follows. The intricate force-chain network of firn induces a multitude of localized lattice preferred orientations within small clusters of grains, which together function as a "nearly isotropic noise" that easily outweighs the strain-induced anisotropy driven by the macroscopic stress acting on the firn skeleton. As firn turns into bubbly ice, such a strong "noise" fades away within the stabilization zone, being gradually eclipsed by the prevailing strain-induced anisotropy imposed by the macroscopic stress that drives the ice flow. This stabilization phenomenon may contribute to the sluggish rotation of *c*-axes generally observed in the upper hundreds of metres of polar ice sheets (Castelnau et al., 1996; Durand et al., 2007; Faria et al., 2002; Weikusat et al., 2017).

6 Conclusion

> *We cannot accept anything as granted beyond the first mathematical formulae. Question everything else.*
>
> Maria Mitchell. Quoted by Holmes (2018).

This work presented an analysis of the orientation distribution of slip bands in the upper 850 m of polar ice from the EPICA (European Project for Ice Coring in Antarctica) drilling site in Dronning Maud Land (DML), Antarctica. Circa 12,000 high-resolution micrographs from eight different vertical sections of the EPICA-DML Deep Ice Core, spaced at roughly 100 m depth intervals, have been manually analysed. The micrographs were taken from fresh ice, shortly after drilling, to avoid undesirable relaxation effects.

The analysis revealed two distinct evolution regimes in the orientation distribution of slip bands. In the shallow bubbly ice beneath the firn–ice transition (viz. pore close-off depth ≈ 88 m) down to a reversal zone at (415 ± 60) m depth, the slip-band orientation distribution evolves from nearly random to one with a strong mid-angle (30–60°) mode. In contrast, below the reversal zone and down to the end of the depth range considered here (853 m), the slip-band orientation distribution becomes strongly unimodal, with a well-defined low-angle (0–30°) mode, which follows the evolution of the strain-induced anisotropy (*c*-axis preferred orientations) of deep bubbly ice.

While the features of the orientation distribution of slip bands below the reversal zone are, as expected, compatible with the *c*-axis anisotropy and the macroscopic stress that drives the large-scale ice flow, the evolution of the distribution of slip bands above the reversal zone turns out to be a puzzling result. In order to explain it, we introduced here the hypothesis of *microstructural fading memory*: force chains, which are characteristic features of the sintering and deformation of granular snow and porous firn, leave mechanical and structural imprints on the microstructure of polycrystalline bubbly ice. These imprints end up affecting the distribution of slip bands at shallow depths, while gradually evanescing under the the action of dynamic recovery and recrystallization, and the redistribution of internal stresses. The very heterogeneous strains associated to force chains are also responsible for the generation of a nearly-random orientation distribution of slip bands and *c*-axes in firn, compatible with the one observed here in the shallowest ice sample just beneath the firn–ice transition depth.

The impact and consequences of these results are remarkable. First, the hypothesis of microstructural fading memory is compatible not only with the slip-band observations described here, but also with the notion and role of force chains in snow and firn (Brown, 1980; Gubler, 1978; Kry, 1975; Scapozza and Bartelt, 2003; von Moos et al., 2003; Wakahama, 1960), the observation of dynamic recrystallization in deep firn (Kipfstuhl et al., 2009) and its theoretical explanation in terms of internal stresses (Faria et al., 2014b). Furthermore, it allows the identification of a *stabilization zone* (which coincides with the shallow bubbly ice zone already described), where relics of the once strongly localized mechanical and structural heterogeneities of ancient firn are gradually dissipated. Whereas this stabilization manifests itself most clearly in the evolution of slip bands reported here, it may also be noticeable in other microstructural features of shallow bubbly ice, including the sluggish evolution of *c*-axis orientations often observed in this zone (Castelnau et al., 1996; Durand et al., 2007; Faria et al., 2002; Weikusat et al., 2017). At last, the observations of slip bands in the anisotropic, deep bubbly ice presented here are compatible with all EPICA-DML studies of ice microstructure and flow performed so far, including grain sizes and elongations, slip bands and subgrain boundaries, visual stratigraphy, *c*-axis preferred orientations and ice-flow simulations (Faria and Kipfstuhl, 2004; Faria et al., 2010, 2014b, 2018; Kipfstuhl et al., 2006; Weikusat et al., 2009, 2017).

Admittedly, the hypothesis of microstructural fading memory and its corollaries are still conjectures open to further scrutiny and corroboration. Following Maria Mitchell's advice quoted at the beginning of this section, we should not accept such conjectures as granted. They are, nevertheless, physically sound and consistent with a number of independent observations of physical phenomena and properties of polar ice, as reported in this work. Therefore, they deserve to be taken seriously, as their value lies also in the new ideas and questions they disclose, which shall promote future investigations of the fascinating phenomenon of firn–ice metamorphism. In this vein, the hypothesis of microstructural fading memory lays the foundations for a new experimental and theoretical framework to study of one of the most important and elusive processes in polar ice: *dynamic recovery.* After accounting for the effects of deformation and recrystallization on the grain stereology, one may use the evolution of slip bands in shallow bubbly ice to estimate the rate at which dislocations disappear from inactive slip bands. This line of research will be pursued in the near future.

Acknowledgements

My gratitude to Sepp Kipfstuhl, Nobuhiko Azuma, and Ilka Weikusat for many discussions and collaboration over the years on the physical properties of polar ice. Special thanks also to Luca Placidi for his excellent guest-editorial work, and to two anonymous reviewers for their invaluable criticism. Financial support from the Ramón y Cajal Grant RYC-2012-12167 of the Spanish Ministry of Economy, Industry and Competitiveness is kindly acknowledged. This work is a contribution to the European Project for Ice Coring in Antarctica (EPICA), a joint European Science Foundation/European Commission scientific programme, funded by the EU and by national contributions from Belgium, Denmark, France, Germany, Italy, the Netherlands, Norway, Sweden, Switzerland and the United Kingdom. The main logistic support was provided by IPEV and PNRA (at Dome C) and AWI (at Dronning Maud Land). This is EPICA publication no. 310.

References

Alley, R. B. (1988). Fabrics in polar ice sheets: development and prediction. *Science*, 240:493–495.

Asaro, R. J. (1983). Micromechanics of crystals and polycrystals. *Adv. Appl. Mech.*, 23:1–115.

Azuma, N. (1994). A flow law for anisotropic ice and its application to ice sheets. *Earth Planet. Sci. Lett.*, 128:601–614.

Azuma, N. and Higashi, A. (1985). Formation processes of ice fabric patterns in ice sheets. *Ann. Glaciol.*, 6:130–134.

Bendel, V., Ueltzhöffer, K. J., Freitag, J., Kipfstuhl, S., Kuhs, W. F., Garbe, C. S., and Faria, S. H. (2013). High-resolution variations in size, number, and arrangement of air bubbles in the EPICA DML ice core. *J. Glaciol.*, 59(217):972–980.

Bernal, J. D. and Fowler, R. H. (1933). A theory of water and ionic solution, with particular reference to hydrogen and hydroxyl ions. *J. Chem. Phys.*, 1(8):515–548.

Brown, R. L. (1980). A volumetric constitutive law for snow based on a neck growth model. *J. Appl. Phys.*, 51(1):161–165.

Bryant, G. W. and Mason, B. J. (1960). Etch pits and dislocations in ice crystals. *Phil. Mag.*, 5(8):1221–1227.

Bunge, H. J. and Schwarzer, R. A. (2001). Orientation stereology—a new branch in texture research. *Adv. Eng. Mater.*, 13(1–2):25–39.

Castelnau, O., Thorsteinsson, T., Kipfstuhl, J., Duval, P., and Canova, G. R. (1996). Modelling fabric development along the GRIP ice core, central Greenland. *Ann. Glaciol.*, 23:194–201.

Clark, P. U., Dyke, A. S., Shakun, J. D., Carlson, A. E., Clark, J., Wohlfarth, B., Mitrovica, J. X., Hostetler, S. W., and McCabe, A. M. (2009). The Last Glacial Maximum. *Science*, 325:710–714.

Durand, G., Gillet-Chaulet, F., Svensson, A., Gagliardini, O., Kipfstuhl, S., Meyssonnier, J., Parrenin, F., Duval, P., and Dahl-Jensen, D. (2007). Change in ice rheology during climate variations—implications for ice flow modelling and dating of the EPICA Dome C core. *Clim. Past*, 3:155–167.

Durham, W. B., Stern, L. A., and Kirby, S. H. (2001). Rheology of ice I at low stress and elevated confining pressure. *J. Geophys. Res.*, 106(6):11031–11042.

Duval, P., Ashby, M. F., and Anderman, I. (1983). Rate-controlling processes in the creep of polycrystalline ice. *J. Phys. Chem.*, 87:4066–4074.

Evans, R. C. (1976). *An Introduction to Crystal Chemistry.* Cambridge University Press, Cambridge, 2nd edition.

Faria, S. H., Freitag, J., and Kipfstuhl, S. (2010). Polar ice structure and the integrity of ice-core paleoclimate records. *Quat. Sci. Rev.*, 29(1):338–351.

Faria, S. H. and Kipfstuhl, S. (2004). Preferred slip band orientations and bending observed in the Dome Concordia (East Antarctica) ice core. *Ann. Glaciol.*, 39:386–390.

Faria, S. H. and Kipfstuhl, S. (2005). Comment on "Deformation of grain boundaries in polar ice" by G. Durand et al. *Europhys. Lett.*, 71(5):873–874.

Faria, S. H., Kipfstuhl, S., and Lambrecht, A. (2018). *The EPICA-DML Deep Ice Core*. Springer, Berlin.

Faria, S. H., Ktitarev, D., and Hutter, K. (2002). Modelling evolution of anisotropy in fabric and texture of polar ice. *Ann. Glaciol.*, 35:545–551.

Faria, S. H., Weikusat, I., and Azuma, N. (2014a). The microstructure of polar ice. Part I: highlights from ice core research. *J. Struct. Geol.*, 61:2–20.

Faria, S. H., Weikusat, I., and Azuma, N. (2014b). The microstructure of polar ice. Part II: state of the art. *J. Struct. Geol.*, 61:21–49.

Glen, J. W. (1968). The effect of hydrogen disorder on dislocation movement and plastic deformation of ice. *Phys. Kondens. Mater*, 7:43–51.

Glen, J. W. (1974). The physics of ice. Cold regions science and engineering monograph II C2a, U. S. Army CRREL, Hanover, NH.

Gödert, G. and Hutter, K. (1998). Induced anisotropy in large ice sheets: theory and its homogenization. *Continuum Mech. Thermodyn.*, 13:91–120.

Gubler, H. (1978). Determination of the mean number of bonds per snow grain and of the dependence of the tensile strength of snow on stereological parameters. *J. Galciol.*, 20(83):329–341.

Hobbs, P. V. (1974). *Ice Physics*. Clarendon, Oxford.

Holmes, R. (2018). Maria Mitchell at 200. *Nature*, 558(7710):370–371.

Kipfstuhl, S. (2007). Thick-section images of the EPICA-Dronning-Maud-Land (EDML) ice core. https://doi.org/10.1594/PANGAEA.663141.

Kipfstuhl, S., Faria, S. H., Azuma, N., Freitag, J., Hamann, I., Kaufmann, P., Miller, H., Weiler, K., and Wilhelms, F. (2009). Evidence of dynamic recrystallization in polar firn. *J. Geophys. Res.*, 114:B05204.

Kipfstuhl, S., Hamann, I., Lambrecht, A., Freitag, J., Faria, S. H., Grigoriev, D., and Azuma, N. (2006). Microstructure mapping: A new method for imaging deformation-induced microstructural features of ice on the grain scale. *J. Glaciol.*, 52(178):398–406.

Kry, P. R. (1975). The relationship between the visco-elastic and structural properties of fine-grained snow. *J. Glaciol.*, 14(72):479–500.

Kuroiwa, D. and Hamilton, W. L. (1963). Studies of ice etching and dislocation etch pits. In Kingery, W. D., editor, *Ice and snow: properties, processes, and applications*, pages 34–55. MIT Press, Cambridge, MA.

Lemke, P., Ren, J., Alley, R. B., Allison, I., Carrasco, J., Flato, G., Fujii, Y., Kaser, G., Mote, P., Thomas, R. H., and Zhang, T. (2007). Observations: changes in snow, ice and frozen ground. In Solomon, S., Qin, D., Manning, M., Chen, Z., Marquis, M., Averyt, K. B., Tignor, M., and Miller, H. L., editors, *Climate Change 2007: The Physical Science Basis*, Contribution of Working Group I to the Fourth Assessment Report of the Intergovernmental Panel on Climate Change (IPCC). Cambridge University Press, Cambridge.

McConnel, J. C. (1890). On the plasticity of an ice crystal. *Proc. Roy. Soc. London*, 49(296–301):323–343.

Mullins, W. W. (1957). Theory of thermal grooving. *J. Appl. Phys.*, 28(3):333–339.

Nakaya, U. (1958). The deformation of single crystals of ice. In *IAHS Red Book 47, Physics of the Movement of Ice*, pages 229–240. International Association of Hydrological Sciences.

Nishida, K. and Narita, H. (1996). Three-dimensional observations of ice crystal characteristics in polar ice sheets. *J. Geophys. Res.*, 101(D16):21311–21317.

Pauling, L. (1935). The structure and entropy of ice and of other crystals with some randomness of atomic arrangement. *J. Amer. Chem. Soc.*, 57:2680–2684.

Petrenko, V. F. and Whitworth, R. W. (1999). *Physics of Ice.* Oxford University Press, Oxford.

Placidi, L., Faria, S. H., and Hutter, K. (2004). On the role of grain growth, recrystallization, and polygonization in a continuum theory for anisotropic ice sheets. *Ann. Glaciol.*, 39:49–52.

Placidi, L., Greve, R., Seddik, H., and Faria, S. H. (2010). Continuum-mechanical, anisotropic flow model, based on an anisotropic flow enhancement factor (CAFFE). *Continuum Mech. Thermodyn.*, 22(3):221–237.

Placidi, L., Hutter, K., and Faria, S. H. (2006). A critical review of the mechanics of polycrystalline polar ice. *GAMM-Mitt.*, 29(1):80–117.

Ruth, U., Barnola, J. M., Beer, J., Bigler, M., Blunier, T., Castellano, E., Fischer, H., Fundel, F., Huybrechts, P., Kaufmann, P., Kipfstuhl, S., Lambrecht, A., Morganti, A., Oerter, H., Parrenin, F., Rybak, O., Severi, M., Udisti, R., Wilhelms, F., and Wolff, E. (2007). "EDML1": a chronology for the EPICA deep ice core from Dronning Maud Land, Antarctica, over the last 150 000 years. *Clim. Past*, 3:475–484.

Scapozza, C. and Bartelt, P. A. (2003). The influence of temperature on the small-strain viscous deformation mechanics of snow: a comparison with polycrystalline ice. *Ann. Glaciol.*, 37:90–96.

Schindelin, J., Arganda-carreras, I., Frise, E., Kaynig, V., Longair, M., Pietzsch, T., Preibisch, S., Rueden, C., Saalfeld, S., Schmid, B., Tinevez, J.-Y., White, D. J., Hartenstein, V., Eliceiri, K., Tomancak, P., and Cardona, A. (2012). Fiji: an open-source platform for biological-image analysis. *Nature Methods*, 9(7):676–682.

Steinhage, D. (2001). Contributions of geophysical measurements in Dronning Maud Land, Antarctica, locating an optimal drill site for a deep ice core drilling. Reports on polar and marine research (ber. polarforsch. meeresforsch.), Alfred Wegener Institute for Polar and Marine Research, Bremerhaven.

Ueltzhöffer, K. J., Bendel, V., Freitag, J., Kipfstuhl, S., Wagenbach, D., Faria, S. H., and Garbe, C. S. (2010). Distribution of air bubbles in the EDML and EDC ice cores from a new method of automatic image analysis. *J. Glaciol.*, 56(196):339–348.

Vaughan, D. G., Comiso, J. C., Allison, I., Carrasco, J., Kaser, G., Kwok, R., Mote, P., Murray, T., Paul, F., Ren, J., Rignot, E., Solomina, O., Steffen, K., and Zhang, T. (2013). Observations: cryosphere. In Stocker, T. F., Qin, D., Plattner, G.-K., Tignor, M., Allen, S., Boschung, J., Nauels, A., Xia, Y., Bex, V., and Midgley, P., editors, *Climate Change 2013: The Physical Science Basis*, Contribution of Working Group I to the Fifth Assessment Report of the Intergovernmental Panel on Climate Change (IPCC). Cambridge University Press, Cambridge.

von Moos, M., Bartelt, P. A., Zweidler, A., and Bleiker, E. (2003). Triaxial tests on snow at low strain rate. Part I. Experimental device. *J. Glaciol.*, 49(164):81–90.

Wakahama, G. (1960). Internal strain and changes in the microscopic texture of snow caused by compression1. compression of a thin section of snow by a static load. *Low Temp. Sci. A*, 19:37–71. In Japanese with English summary.

Wang, Y., Kipfstuhl, S., Azuma, N., Thorsteinsson, T., and Miller, H. (2003). Ice-fabrics study in the upper 1500 m of the Dome C (East Antarctica) deep ice core. *Ann. Glaciol.*, 37:97–104.

Weikusat, I., Jansen, D., Binder, T., Eichler, J., Faria, S. H., Wilhelms, F., Kipfstuhl, S., Sheldon, S., Miller, H., Dahl-Jensen, D., and Kleiner, T. (2017). Physical analysis of an Antarctic ice core—towards an integration of micro- and macrodynamics of polar ice. *Phil. Trans. R. Soc. A*, 375(2086):20150347.

Weikusat, I., Kipfstuhl, S., Faria, S. H., Azuma, N., and Miyamoto, A. (2009). Subgrain boundaries and related microstructural features in EDML (Antarctica) deep ice core. *J. Glaciol.*, 55(191):461–472.

Wilhelms, F., Miller, H., Gerasimoff, M. D., Drücker, C., Frenzel, A., Fritzsche, D., Grobe, H., Hansen, S. B., Hilmarsson, S. Æ., Hoffmann, G., Hörnby, K., Jaeschke, A., Jakobsdóttir, S. S., Juckschat, P., Karsten, A., Karsten, L., Kaufmann, P. R., Karlin, T., Kohlberg, E., Kleffel, G., Lambrecht, A., Lambrecht, A., Lawer, G., Schärmeli, I., Schmitt, J., Sheldon, S. G., Takata, M., Trenke, M., Twarloh, B., Valero-Delgado, F., and Wilhelms-Dick, D. (2014). The EPICA Dronning Maud Land deep drilling operation. *J. Glaciol.*, 55(68):355–366.

Woodcock, N. H. (1977). Specification of fabric shapes using an eigenvalue method. *Geol. Soc. Amer. Bull.*, 88:1231–1236.

Table 1: EPICA-DML ice-core samples selected for this study. Age estimates from Ruth et al. (2007).

No.	Depth (m)	Age (ka BP)	Anisotropy	Description
1	94	0.93	nearly isotropic†	shallow bubbly ice just beneath the pore close-off depth
2	205	2.56	nearly isotropic†	shallow bubbly ice
3	355	4.95	nearly isotropic†	shallow bubbly ice
4	473	7.14	slightly orthotropic	deep bubbly ice
5	555	8.83	fairly orthotropic	deep bubbly ice
6	655	11.0	orthotropic	deep bubbly ice
7	755	13.4	orthotropic	deep bubbly ice
8	854	16.0	orthotropic	deep bubbly ice on top of the bubble–hydrate transition zone

†All nearly isotropic samples have a Woodcock strength parameter $C \approx 0.5$ (cf. Woodcock 1977).

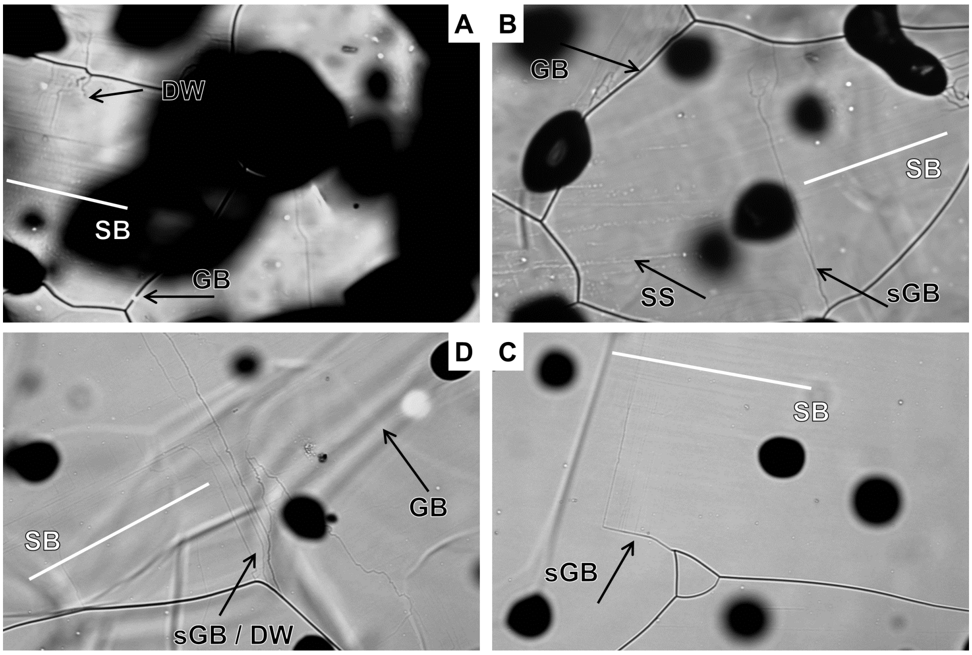

Figure 1: Examples of real slip bands and other features that resemble them. Real slip bands are indicated by white lines and the text "SB". Other structures are indicated by black arrows with the following meanings: GB = grain boundary; sGB = subragin boundary, SS = surface scratch, DW = dislocation wall. Each micrograph measures 2.5×1.8 mm. The sample depths are (A) 94 m. (B) 205 m. (C) and (D) 555 m.

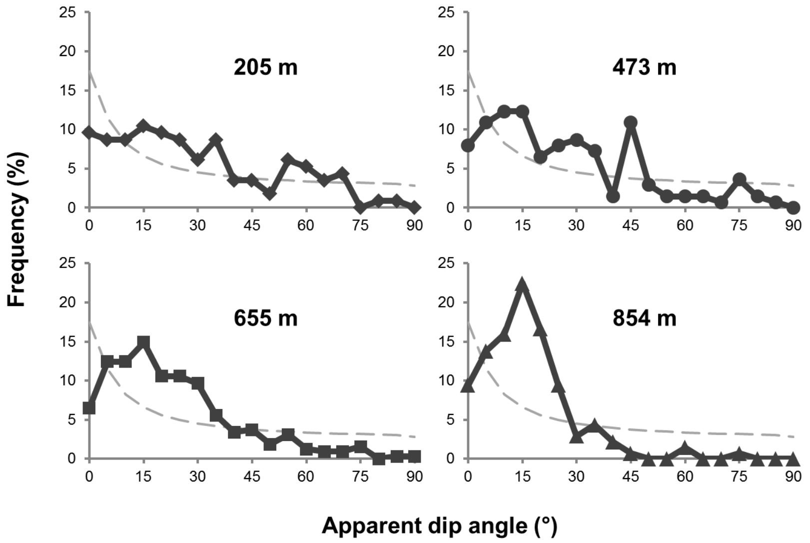

Figure 2: Examples of orientation distribution of slip bands of the even-numbered samples (the odd-numbered samples tell essentially the same story). The dashed grey lines describe a reference distribution of the ideal case of randomly oriented slip bands, taking into account the effects derived from Remarks 1 and 2.

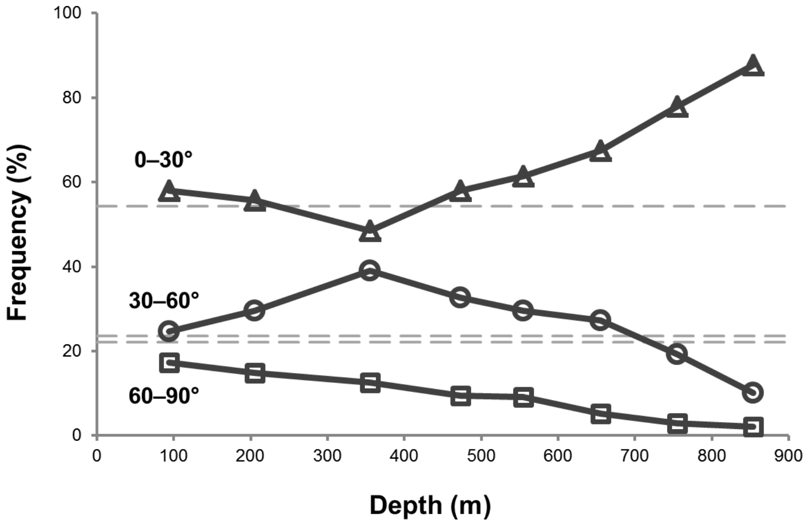

Figure 3: Evolution with depth (and age) of low- (0–30°), mid- (30–60°), and high-angle (60–90°) dip classes of slip bands. The dashed grey lines serve as reference to the frequencies of low-, mid-, and high-angle dip classes in the ideal case of randomly oriented slip bands, taking into account the effects derived from Remarks 1 and 2.